

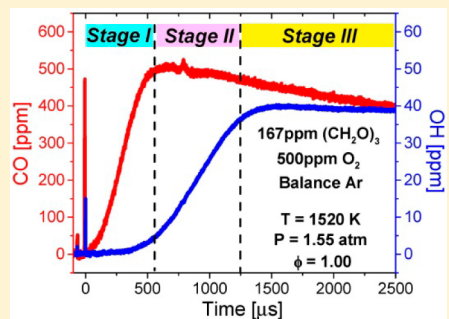
Shock Tube and Laser Absorption Study of CH₂O Oxidation via Simultaneous Measurements of OH and CO

Shengkai Wang,*^{ID} David F. Davidson,^{ID} and Ronald K. Hanson

High Temperature Gasdynamics Laboratory, Stanford University, Stanford, California 94305, United States

S Supporting Information

ABSTRACT: The oxidation of Ar-diluted stoichiometric CH₂O–O₂ mixtures was studied behind reflected shock waves over temperatures of 1332–1685 K, at pressures of about 1.5 atm and initial CH₂O mole fractions of 500, 1500, and 5000 ppm. Quantitative and time-resolved concentration histories of OH and CO (at both $\nu'' = 0$ and $\nu'' = 1$) were measured by narrow-linewidth laser absorption at 306.7 and 4854 nm, respectively. A time delay was observed between the formation of $\nu'' = 0$ and $\nu'' = 1$ states of CO, suggesting that CO was kinetically generated primarily in the ground state and then collisionally relaxed toward vibrational equilibrium. The measured CO and OH time-histories were used to evaluate the performance of four detailed reaction mechanisms regarding the oxidation chemistry of CH₂O. Further analyses of these time-history data have also led to improved determination for the rate constants of two key reactions, namely H + O₂ = O + OH (R1) and OH + CO = CO₂ + H (R2), as follows: $k_1 = 8.04 \times 10^{13} \exp(-7370 \text{ K}/T) \text{ cm}^3 \text{ mol}^{-1} \text{ s}^{-1}$, $k_2 = 1.90 \times 10^{12} \exp(-2760 \text{ K}/T) \text{ cm}^3 \text{ mol}^{-1} \text{ s}^{-1}$; both expressions are valid over 1428–1685 K and have 1σ uncertainties of approximately $\pm 10\%$.



INTRODUCTION

Present in the oxidation of virtually all hydrocarbons and oxygenated fuels, formaldehyde, CH₂O, is a key intermediate species in gas phase hydrocarbon combustion systems. During combustion, a significant fraction of carbon in the fuel is converted into CH₂O before eventually being oxidized to CO and CO₂. As a partial oxidation product, CH₂O is not only a critical benchmark of the overall combustion progress, but also a fundamental building block of combustion kinetics models. Hydrocarbon combustion models are conventionally developed in a bottom-up manner,¹ with H₂/O₂ chemistry being the very foundation of the hierarchy and large hydrocarbons being at the top of the structure, and the reactions of C₁ species (CO, CH₂O, CH₃OH, CH₄, etc.) providing an interface. Notably, recently advocated top-down modeling approaches also require an accurate C₀–C₄ base mechanism,^{2,3} of which CH₂O chemistry is an important component.

Because of its essential role in hydrocarbon combustion chemistry, CH₂O has attracted intense research attention over the last few decades. The pyrolysis and oxidation of CH₂O have been experimentally studied in static^{4–6} and flow reactors,^{7–11} flames,^{12–17} and shock tubes,^{18–32} using a variety of diagnostic methods such as pressure,^{4–6} gas chromatography (GC),^{5,6,8,9,14} mass spectrometry (MS),^{12,13,15,17} Fourier-transform infrared spectroscopy (FTIR),¹¹ laser-induced fluorescence,¹⁴ laser schlieren,²⁶ and emission^{14,19–22,27} and absorption spectroscopy.^{19,22–25,27–32} Among various experimental data obtained from these studies, quantitative and time-resolved species concentration histories are especially valuable for validating modern combustion models.³³ However, direct

CH₂O oxidation data are very scarce in the literature. Particularly, no simultaneous OH and CO concentration measurements have been previously reported. Both species contain key information on CH₂O oxidation chemistry: OH is the carrier of chain branching and propagation reactions and reflects the overall reactivity of the system, whereas CO tracks the distribution of carbon atoms. Hence we were motivated to perform the first simultaneous OH and CO time-history measurements during stoichiometric oxidation of CH₂O.

EXPERIMENTAL METHOD

Formaldehyde oxidation experiments were performed in a high-purity shock tube of 14.13 cm inner diameter at Stanford University. The shock tube has a driver section of 3.3 m and a driven section of 8.5 m, which allowed for steady test times of 2–2.5 ms under the conditions of the current study. Measurements were taken behind the reflected shock waves, where the initial gas temperatures and pressures were determined from the incident shock speed at the endwall location, using ideal shock relations. The incident shock velocities were calculated from the time intervals between the arrivals of incident shock waves at 5 PCB piezoelectric pressure transducers located on the sidewall over the last 1.5 m of the shock tube, and then linearly extrapolated to the endwall location. The uncertainties in temperatures and pressures (less than $\pm 0.5\%$) were mainly due to uncertainties in the measured

Received: September 20, 2017

Revised: October 24, 2017

Published: October 25, 2017

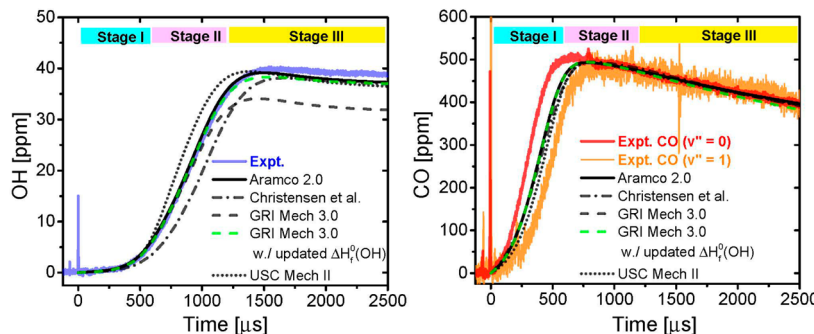


Figure 1. Example OH (left panel) and total CO (right panel) time-histories in comparison with numerical simulations with different mechanisms. Initial condition after the reflected shock wave: $T = 1520$ K, $P = 1.55$ atm, and 167 ppm of 1,3,5-trioxane/500 ppm of O₂/Ar. A 1.5 ppm initial H impurity was added in the simulations to match the observed timing of the OH rise. Note, however, that this H impurity does not affect the slopes of OH formation and CO removal.

shock velocities ($\pm 0.2\%$). Further details about this Stanford shock tube facility can be found in our previous work.³⁴

Test gas mixtures were manometrically prepared in a stainless-steel mixing tank that was preheated to 50 °C to prevent wall condensation. Research grade 1,3,5-trioxane (>99% purity, supplied by Sigma-Aldrich) was used as a pyrolytic precursor for CH₂O. When shock-heated at $T > 1000$ K, 1,3,5-trioxane decomposes almost instantaneously, producing three parts of CH₂O with little byproducts.³⁵ The 1,3,5-trioxane was vaporized and mixed with high-purity O₂ and Ar (>99.99% and >99.999%, respectively; both supplied by Praxair). For preparing test mixtures of less than 1000 ppm trioxane, a double-dilution method was used, following the procedure described in our previous work,³⁴ in order to achieve more accurate control of the mixture composition.

Time-resolved species mole fraction histories were measured behind reflected shock waves using laser absorption diagnostics through two pairs of optical ports located 2 cm away from the shock tube endwall. The CO time-histories were measured using mid-IR laser absorption at 4854.58 nm (2059.91 cm⁻¹) and 4853.59 nm (2060.33 cm⁻¹), targeting the P(20) transition of the CO ($v' = 1 \leftarrow v'' = 0$) band and the P(14) transition of the ($v' = 2 \leftarrow v'' = 1$) band, respectively. The OH time-histories were measured using UV laser absorption at 306.7 nm (32606.53 cm⁻¹), targeting the peak of the R₁(S) transition of the OH A-X (0,0) band. The species time-history data were extracted from the absorption signal via the Beer-Lambert relation, $\alpha = -\ln(I/I_0) = \chi\sigma nL$, where α was the absorbance calculated from the logarithmic ratio of the transmitted and incident laser intensities I and I₀, χ was the mole fraction of the absorbing gas, σ was its absorption cross-section, n was the total number density of the test gas, and L was the optical path-length (14.13 cm). Absorption cross sections of CO and OH were obtained from previous studies by Ren et al.³⁶ and Herbon et al.,³⁷ respectively.

It is worth noting that CH₂O also absorbs at the UV wavelength, as investigated in our previous study.³¹ However, its absorption contribution was very small compared to that of OH (less than 1% of the peak OH absorbance). Nonetheless, we have corrected for this effect by subtracting the interference absorption of CH₂O, whose concentration time-histories were determined via carbon balance from the CO measurement. No interference absorption was expected at the two mid-IR wavelengths of CO measurement.

RESULTS AND DISCUSSION

In the following sections, we will discuss the results of the current study in two steps. First, we will report our OH and CO time-history measurements and use them to evaluate the performance of four comprehensive reaction models regarding the oxidation chemistry of CH₂O. Then we will discuss our improved determination for the rate constants of two key reactions, H + O₂ = O + OH (R1) and OH + CO = CO₂ + H (R2), based on further analyses of these time-history data.

OH and CO Time-Histories. Figure 1 shows the example measurement for the stoichiometric oxidation of 500 ppm of CH₂O at 1520 K, 1.55 atm. A three-stage behavior is clearly observed from the evolution of OH and CO time-histories: stage I (approximately 0–600 μs in this example) corresponds to the decomposition of CH₂O into HCO and its subsequent conversion into CO and H₂; stage II (approximately 600–1200 μs) corresponds to H₂ oxidation; and stage III (approximately 1200 μs to the end of test time) corresponds to the conversion of CO into CO₂. Multiple kinetics targets could be extracted from these time-history measurements for evaluating and calibrating modern reaction models. The current study particularly focuses on the slopes of OH formation and CO depletion and the peak OH concentration.

In comparison with the measurement results, also shown in Figure 1 are the predictions of four comprehensive reaction mechanisms, namely Aramco 2.0,³⁸ GRI Mech 3.0,³⁹ USC Mech II,⁴⁰ and a very recent mechanism from Christensen et al.⁴¹ All these mechanisms, except GRI Mech 3.0, are seen to decently recover the peak concentration of OH; GRI Mech 3.0, on the other hand, substantially underpredicts the OH concentration, which we suspect is caused by the outdated value of $\Delta H_f^0(\text{OH})$ used in the mechanism. When updated with the recent $\Delta H_f^0(\text{OH})$ value from Ruscic et al.⁴² and Herbon et al.,⁴³ GRI Mech 3.0 is in much improved agreement with the current measurement. Both Aramco 2.0 and the Christensen mechanism accurately capture the slope of OH formation, while USC Mech II slightly overpredicts the OH slope. All the above four mechanisms are seen to predict the peak concentration and removal rate of CO very well.

Note that in stage I of the previous example, the total CO concentration time-histories inferred from measurements at the ground vibrational state ($v'' = 0$) and the first excited state ($v'' = 1$) (assuming in both cases a vibrational temperature equal to the translational temperature) exhibit an offset of about 200 μs. Similar offset has been observed consistently over all experimental conditions of the current study, which suggests

that the CO formation in the current reaction system follows a two-step process, i.e., CO is kinetically generated primarily in the ground state and then collisionally relaxed toward vibrational equilibrium (further analysis of vibrational-state-resolved CO time-histories can be found in the *Supporting Information*). For kinetic modelers who may use time-history data of CO formation as targets for optimizing CH_2O oxidation mechanisms, it is thus crucially important to distinguish between measurements of different vibrational states. For example, emission-based measurements always probe $v'' = 1$ or higher (e.g., Saito et al.²²), whereas absorption-based measurements typically target $v'' = 0$ for optimal detection sensitivity (e.g., the current work), but can also be performed on the excited vibrational states (e.g., Lin et al.²⁴ and Eiteneer et al.²⁵). In the latter case, proper modeling or correction for vibrational relaxation is often required. Additionally, rate constants of CO reactions have been found to be vibrational-state-dependent,^{44,45} therefore a multistate model (e.g., Wooldridge et al.⁴⁵) is recommended for modeling the chemistry of CO in vibrational nonequilibrium. In the current work, however, we primarily focus our analysis on the plateau and depletion regions of CO time-histories (stages II and III) where vibrational equilibrium has been established, and hence we choose to use the conventional state-independent reaction model due to its simplicity.

Care is also advised when one uses the exact timing of CO or OH formation as a kinetic target, as it is sensitive to residual low-level impurities in the shock tube (see Figure 2). A similar

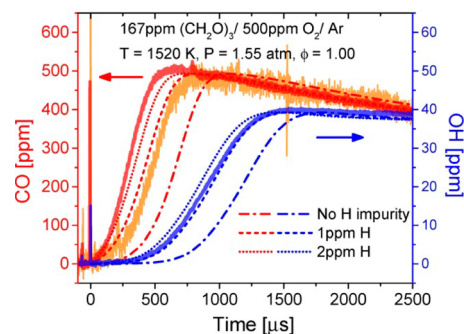


Figure 2. Effect of H impurity on OH and CO time-histories. Simulation performed using the Aramco 2.0 mechanism.³⁸

impurity effect was observed in the H_2 oxidation measurement performed in the same shock tube by Hong et al. in 2011,⁴⁶ and

discussed in detail later in the work of Urzay et al.⁴⁷ These impurities could have possibly resulted from trace amount of hydrocarbons in the Ar bath gas (as noticed in our recent study⁴⁸) or in the 1,3,5-trioxane sample. Following a similar approach as introduced by Hong et al.,⁴⁶ we have estimated the H-impurity level (from the onset time of OH formation) to be 1.5 ppm in this example case. Despite its impact on the timing of OH and CO formation, however, we would like to note that the H impurity affects neither the slopes of the OH and CO profiles nor the peak concentration of OH, which are the primary kinetics targets in this study. In future experiments we intend to use purer Ar and trioxane if available, and to explore additional gas purification techniques to remove small hydrocarbon impurities, for example, with the Zn–V–Fe alloy getter introduced by George et al.⁴⁹

Measurements at higher concentrations of CH_2O have also been performed, as shown in Figure 3a, Figure 3b, Figure 4a, and Figure 4b. These OH and CO time-histories were determined using T, P -dependent absorption cross sections based on the temperature and pressure time-histories simulated with Aramco 2.0, and the maximum measurement uncertainties induced by uncertainties in local temperature (<20 K) and pressure (<0.03 atm) were estimated to be less than 5% in both examples. In these cases the predictions of all four reaction mechanisms examined in the current study begin to diverge from the measurements. In both examples, all mechanisms, except the original GRI Mech 3.0, are seen to slightly overpredict the peak OH concentrations. In the second example (500 ppm of CH_2O oxidation at 1364 K), Aramco 2.0, USC Mech II and GRI Mech 3.0 predict slightly earlier rise time of OH (which is usually defined as the ignition delay time of the system), while the Christensen et al. mechanism predicts a late OH rise time and overpredicts the removal rate of CO. Evidently, the current time-history data (available in the *Supporting Information*) can provide valuable calibration targets for future optimization/improvement of these models.

Rate Constant Determination. The time-history data presented in the previous section contain important kinetic information (e.g., the slopes of OH formation and CO depletion) and merit further analysis. The following analysis is focused on the 500 ppm of CH_2O oxidation cases, in which the use of a dilute CH_2O mixture has minimized temperature and pressure changes and competitions between various reactions, allowing extraction of individual reaction rate constants. For example, sensitivity analysis (Figure 5a) suggests that in stage II the OH time-histories are dominated by the

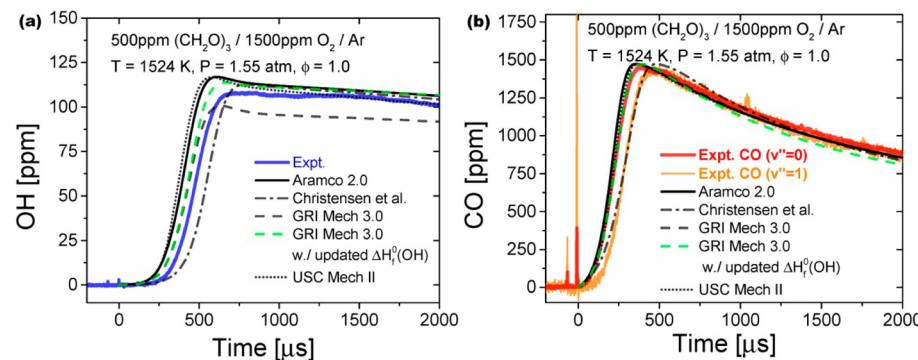


Figure 3. Example time-histories of (a) OH and (b) CO in stoichiometric oxidation of 1500 ppm of CH_2O . Initial condition after the reflected shock wave: $T = 1524 \text{ K}$, $P = 1.55 \text{ atm}$, and 500 ppm of 1,3,5-trioxane/1500 ppm of O_2/Ar . A 1.5 ppm initial H impurity was added in the simulations.

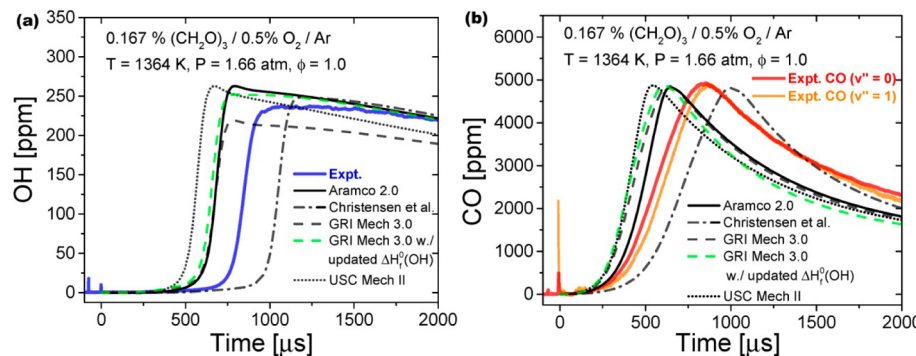


Figure 4. Example time-histories of (a) OH and (b) CO in stoichiometric oxidation of 5000 ppm of CH_2O . Initial condition after the reflected shock: $T = 1364 \text{ K}$, $P = 1.66 \text{ atm}$, and 0.167% 1,3,5-trioxane/0.5% O_2/Ar . The influence of H impurity was expected to be insignificant at this condition; therefore, no H impurity was added in these simulations.

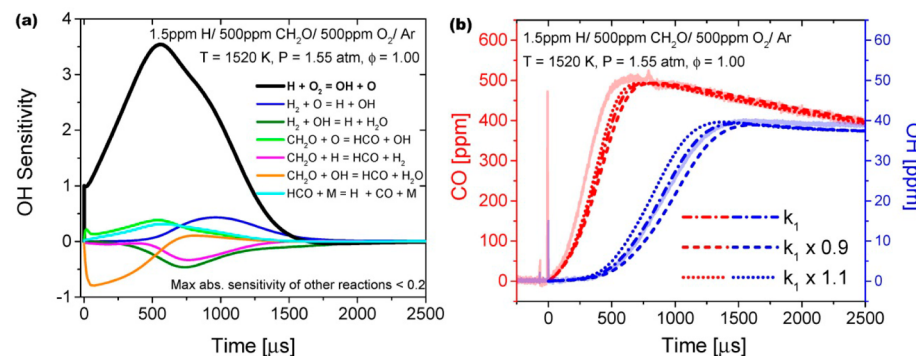


Figure 5. Kinetic analysis for stage II of CH_2O oxidation. (a) Normalized sensitivity, $S_{\text{OH},i}(t) = \partial[\ln [\text{OH}](t)]/\partial[\ln k_i]$, of the OH time-history. Note that the reaction of $\text{H} + \text{O}_2 = \text{OH} + \text{O}$ (R1) dominates the OH sensitivity in stage II. (b) Effect of k_1 on OH and CO time-histories. Simulation was performed using Aramco 2.0.³⁸

reaction of $\text{H} + \text{O}_2 = \text{OH} + \text{O}$ (R1). The OH formation rate is very sensitive to k_1 : as Figure 5b clearly indicates, perturbing k_1 by even 10% would significantly affect the slope of OH formation. The CO time-histories, on the other hand, exhibit little sensitivity to k_1 in stage II and III, as varying k_1 would only slightly shift the CO trace without affecting the CO removal rate.

It was thus possible to infer an improved value of k_1 from the current OH measurement. This analysis was assisted by numerical simulation using a detailed reaction mechanism, Aramco 2.0,³⁸ and the value of k_1 was determined by best-fitting the simulated OH time-history to the measurement within its 10–90% rise period. To account for the influence of H-impurity in the shock tube (time-shifting of the OH-time history), we also included in the simulation some initial H radical, whose concentration was treated as unknown. During this analysis, k_1 and $[\text{H}]_0$ were varied independently, and the optimal pair of (k_1 , $[\text{H}]_0$) that yielded the minimum root-mean-squared (RMS) residual fitting error (e_{OH}) was selected. From the fitting we have also estimated the posterior probability distribution function (PDF) and fitting uncertainty of k_1 and $[\text{H}]_0$, as illustrated in Figure 6. The posterior PDF was obtained from Bayesian statistics:

$$p(k_1, [\text{H}]_0 | \text{OH data}) \propto \exp\{-[e_{\text{OH}}(k_1, [\text{H}]_0)]^2 / 2\sigma_{\text{OH}}^{-2}\} \quad (1)$$

where σ_{OH} was the 1σ detection limit of OH concentration calculated from the minimum detectable absorbance (1×10^{-3}) measured in nonreactive shock experiments; no prior knowl-

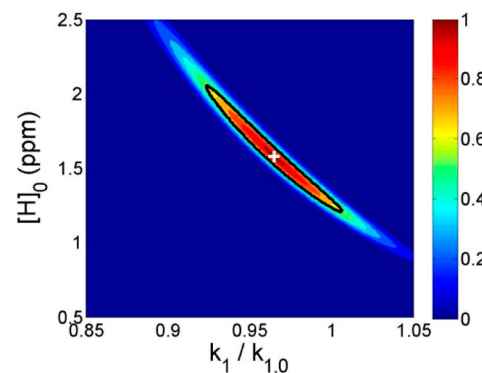


Figure 6. Peak-normalized posterior PDF of $([\text{H}]_0, k_1)$ inferred from the OH time-history in the 1520 K, 1.55 atm, 167 ppm 1,3,5-trioxane/500 ppm of O_2/Ar example. k_1 is normalized by the original value ($k_{1,0}$) in Aramco 2.0.³⁸ The black line indicates the 1σ uncertainty bound.

edge of $(k_1, [\text{H}]_0)$ was assumed. The typically 1σ fitting uncertainty for k_1 was found to be about $\pm 4\%$.

Aside from the fitting uncertainty, other factors were also included in our detailed uncertainty analysis for k_1 , as shown in Figure 7. All uncertainty sources that could affect the inferred value of k_1 by more than $\pm 1\%$ were considered in this analysis, including: fitting uncertainty of about $\pm 4\%$; uncertainties in the OH absorption cross-section ($\pm 3\%$, obtained from Rea et al.⁵⁰ and Herbon et al.³⁷) and in the mixture composition (estimated to be $\pm 3\%$); uncertainty in the nominal reflected shock temperature ($\pm 7 \text{ K}$, which translates to about $\pm 2\%$ uncertainty

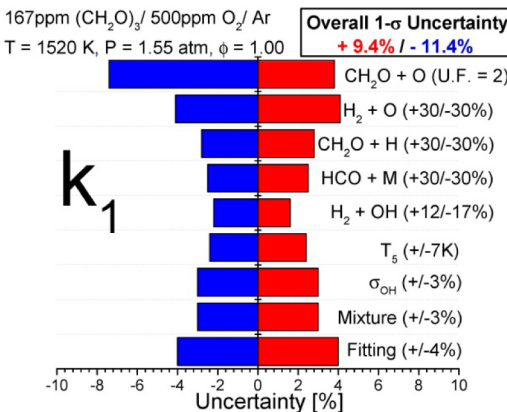


Figure 7. Uncertainty analysis for the value of k_1 inferred from the previous example.

in k_1); and uncertainties in the rate constants of a few secondary reactions (values obtained from their source literature^{26,28,51–53}). The overall (root-sum-squared) 1 σ uncertainty of k_1 was calculated to be +9%/-11%.

The best-fit values of k_1 and their uncertainties have been summarized in Table 1. Over the temperature range of the current study (1428–1520 K), k_1 can be expressed in an Arrhenius form as $k_1 = 8.04 \times 10^{13} \exp(-7370 \text{ K}/T) \text{ cm}^3 \text{ mol}^{-1} \text{ s}^{-1}$. The current results are compared with previous studies, as illustrated in Figure 8. Within their overlapping temperature range, the current results are seen to be in excellent agreement with the previous data reported by Hong et al.⁴⁶ Additionally, however, the current study has provided k_1 data at higher temperatures. Also included in this comparison are analytical expressions for k_1 used in several representative reaction models. For example, Aramco 2.0³⁸ and the Christensen et al. model⁴² adopted the best-fit Arrhenius expression of Hong et al., which agrees very well with the current results at the low temperature end; FFCM-1,⁵⁴ a recently available foundational fuel chemistry model, employed a k_1 expression that agrees better with the current data at the high temperature end; the earlier GRI Mech 3.0³⁹ and USC Mech II⁴⁰ mechanisms used slightly higher k_1 than reported in the current and the Hong et al. studies.

Similarly, the rate constant of $\text{CO} + \text{OH} = \text{CO}_2 + \text{H}$ (R2), k_2 , can be inferred from the CO removal rate in stage III. As shown in Figure 9a, the CO sensitivity in stage III is dominated by R1 and R2. Given that k_1 has been determined in the previous section, the rate constant k_2 can thus be obtained by best-fitting the measured stage III CO time-histories (specifically, in the region between 90% OH peak and the end of test time) with numerical simulations, again using Aramco 2.0³⁸ as the base mechanism. In the current study we have conducted a thorough analysis for the joint probability distribution of (k_2, k_1) . Assuming that the noise in the OH and CO time-history data

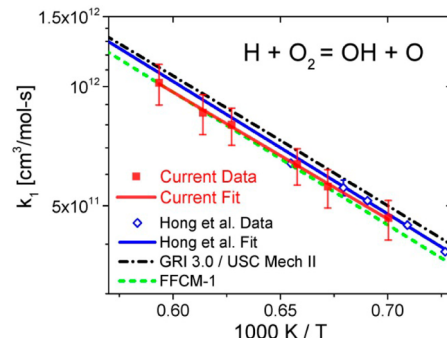


Figure 8. Arrhenius diagram of current vs previous values of k_1 . Error bars denote 1 σ uncertainty of the measurements.

are independent, we have combined our knowledge of k_1 and $[\text{H}]_0$ obtained previously from the OH time-histories, and calculated the posterior PDF of $(k_2, k_1, [\text{H}]_0)$ based on the joint fitting-errors (e_{CO} , e_{OH}):

$$\begin{aligned} p(k_2, k_1, [\text{H}]_0 | \text{OH data}, \text{CO data}) \\ = p(k_2, k_1, [\text{H}]_0 | \text{CO data}) p(k_1, [\text{H}]_0 | \text{OH data}) \\ \propto \exp\{-[e_{\text{CO}}(k_2, k_1, [\text{H}]_0)]^2 / 2\sigma_{\text{CO}}^{-2}\} \\ \exp\{-[e_{\text{OH}}(k_1, [\text{H}]_0)]^2 / 2\sigma_{\text{OH}}^{-2}\} \end{aligned} \quad (2)$$

where the 1 σ detection limit of CO mole fraction, σ_{CO} , is about 4 ppm. The joint posterior PDF of (k_2, k_1) is then calculated by marginalizing/integrating over $[\text{H}]_0$, i.e.

$$\begin{aligned} p(k_2, k_1 | \text{OH data}, \text{CO data}) \\ = \int p(k_2, k_1, [\text{H}]_0 | \text{OH data}, \text{CO data}) d[\text{H}]_0 \end{aligned} \quad (3)$$

The result is shown in Figure 10. Note that the posterior probability distributions of k_2 and k_1 are essentially independent, which agrees with our expectation because varying k_1 would not change the slopes of CO removal in stage III (see Figure 5b). Hence the uncertainty in k_1 does not propagate to k_2 .

A detailed uncertainty analysis for k_2 is shown in Figure 11. The overall 1 σ uncertainty of k_2 was calculated to be $\pm 9\%$, most of which was induced by uncertainties in fitting, mixture composition, CO absorption cross-section and the reflected shock temperature; influences of secondary reactions and H-impurity were found to be negligible (uncertainty contributions less than $\pm 1\%$) in the determination of k_2 . The best-fit values of k_2 and their uncertainties have been reported in Table 1, and an Arrhenius fit over the current temperature range yields $k_2 = 1.90 \times 10^{12} \exp(-2760 \text{ K}/T) \text{ cm}^3 \text{ mol}^{-1} \text{ s}^{-1}$. These results are compared with previous studies in Figure 12. The current data are seen to agree with the previous measurements of Wooldridge et al.⁴⁵ within their respective error bars and

Table 1. Rate Constant Values Inferred from the Current Measurements

| T [K] | P [atm] | k_1 [$\text{cm}^3/\text{mol}\cdot\text{s}$] | 1 σ uncert. [%] | k_2 [$\text{cm}^3/\text{mol}\cdot\text{s}$] | 1 σ uncert. [%] |
|-------|---------|---|------------------------|---|------------------------|
| 1428 | 1.65 | 4.66×10^{11} | +10.7/-12.0 | 2.79×10^{11} | +9.1/-9.1 |
| 1488 | 1.58 | 5.59×10^{11} | +10.3/-11.7 | 2.66×10^{11} | +8.2/-8.2 |
| 1520 | 1.55 | 6.36×10^{11} | +9.4/-11.4 | 3.38×10^{11} | +8.7/-8.7 |
| 1594 | 1.53 | 8.01×10^{11} | +10.0/-11.3 | 3.39×10^{11} | +8.2/-8.2 |
| 1629 | 1.50 | 8.59×10^{11} | +10.9/-12.0 | 4.47×10^{11} | +8.2/-8.2 |
| 1685 | 1.46 | 1.02×10^{12} | +11.2/-12.2 | 4.62×10^{11} | +8.1/-8.1 |

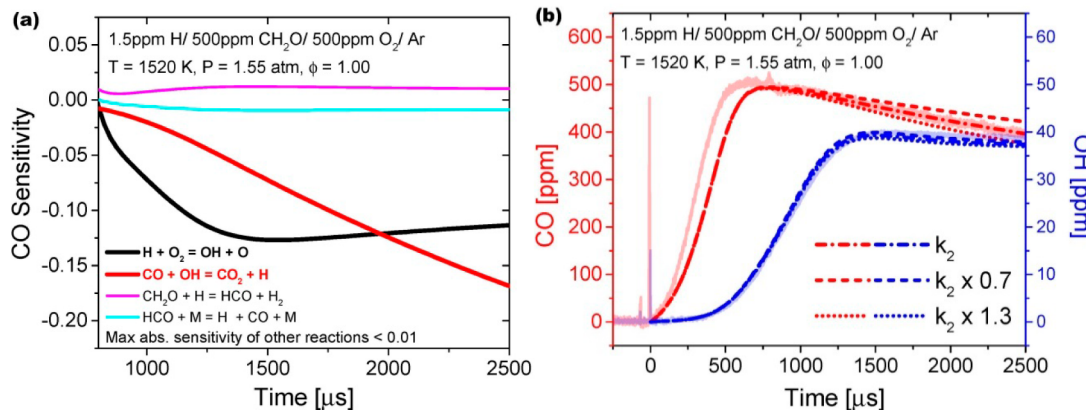


Figure 9. Kinetic analysis for stage III of CH_2O oxidation. (a) Normalized sensitivity, $S_{CO,i}(t) = \partial[\ln [CO](t)]/\partial[\ln k_i]$, of the CO time-history in stage III. (b) Effect of k_2 on OH and CO time-histories. Simulation was performed using Aramco 2.0.³⁸

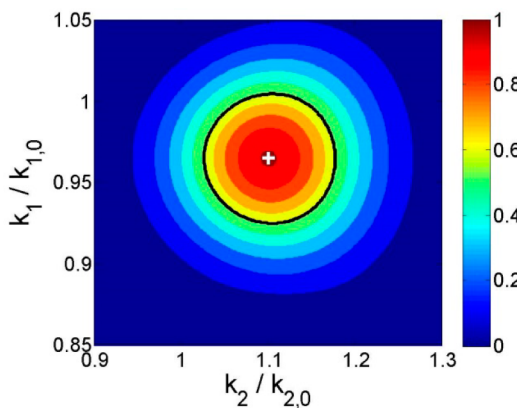


Figure 10. Peak-normalized posterior PDF of (k_1, k_2) inferred from the CO and OH time-histories in the 1520 K, 1.55 atm, and 167 ppm of 1,3,5-trioxane/500 ppm of O_2/Ar example. The black line indicates the 1σ uncertainty bound.

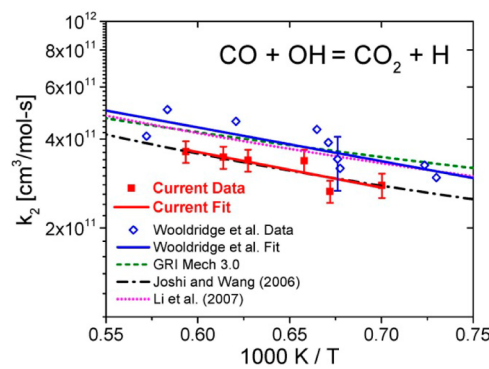


Figure 12. Arrhenius diagram of current vs previous values of k_2 . Error bars denote the 1σ uncertainty of the measurements.

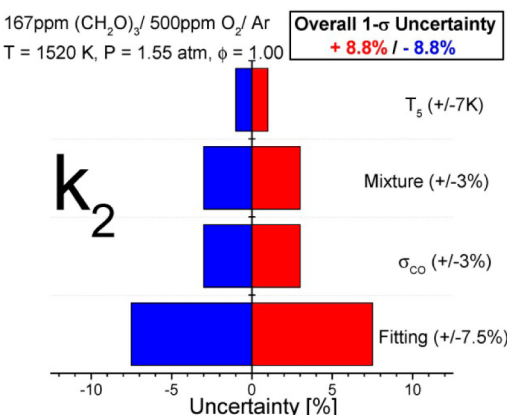


Figure 11. Uncertainty analysis for the value of k_2 inferred from the previous example.

exhibit less scatter. The minor difference between the mean values of the two studies was possibly due to the use of an outdated value of $\Delta H_f^0(OH)$ in the Wooldridge et al. work. The theoretical calculation by Joshi and Wang³⁵ agrees very closely with the current study, whereas values from GRI Mech 3.0³⁹ and the Li et al. model¹¹ are slightly higher (by about 20%) than the current results.

CONCLUSIONS

In this study, we performed simultaneous measurements for OH and CO ($v'' = 0$ and 1) time-histories in oxidation experiments of stoichiometric Ar-diluted CH_2O-O_2 mixtures. From these measurements we inferred improved rate constant determinations for two key reactions, $H + O_2 = OH + O$ and $CO + OH = CO_2 + H$. The results from this study should also provide unique kinetic targets for testing, validating, and improving detailed reaction mechanisms involving CH_2O chemistry. Future work will focus on investigating other key reactions (e.g., reactions involving HCO and O atoms) in the CH_2O oxidation system and extending time-history measurements to other species, such as H_2O , CO_2 , and HCO.

ASSOCIATED CONTENT

Supporting Information

The Supporting Information is available free of charge on the ACS Publications website at DOI: [10.1021/acs.jpca.7b09362](https://doi.org/10.1021/acs.jpca.7b09362).

Data and analysis of vibrational-state-resolved CO time-histories (PDF)

OH and CO time-history data measured during the stoichiometric oxidation of 500, 1500, and 5000 ppm of CH_2O with Ar dilution (PDF)

AUTHOR INFORMATION

Corresponding Author

*(S.W.) E-mail: sk.wang@stanford.edu.

ORCID®

Shengkai Wang: 0000-0003-0947-4643

David F. Davidson: 0000-0002-4470-0135

Notes

The authors declare no competing financial interest.

ACKNOWLEDGMENTS

This material is based upon work supported by the National Science Foundation under Grant No. CBET-1508748.

REFERENCES

- (1) Metcalfe, W. K.; Burke, S. M.; Ahmed, S. S.; Curran, H. J. A. Hierarchical and Comparative Kinetic Modeling Study of C₁–C₂ Hydrocarbon and Oxygenated Fuels. *Int. J. Chem. Kinet.* **2013**, *45*, 638–675.
- (2) Xu, R.; Wang, H.; Hanson, R. K.; Davidson, D. F.; Bowman, C. T.; Egolfopoulos, F. N. Evidence Supporting a Simplified Approach to Modeling High-Temperature Combustion Chemistry. In *10th US National Meeting on Combustion*; College Park, MD, April 2017.
- (3) Wang, K.; Xu, R.; Parise, T.; Shao, J. K.; Lee, D. J.; Movaghfar, A.; Davidson, D. F.; Hanson, R. K.; Wang, H.; Bowman, C. T., et al. Combustion Kinetics of Conventional and Alternative Jet Fuels using a Hybrid Chemistry (HyChem) Approach. In *10th US National Meeting on Combustion*; College Park, MD, April 2017.
- (4) Baldwin, R. R.; Cowe, D. W. The Inhibition of the Hydrogen+Oxygen Reaction by Formaldehyde. *Trans. Faraday Soc.* **1962**, *58*, 1768–1781.
- (5) Baldwin, R. R.; Fuller, A. R.; Longthorn, D.; Walker, R. W. Addition of Formaldehyde to Slowly Reacting Hydrogen+Oxygen Mixtures. *J. Chem. Soc., Faraday Trans. 1* **1972**, *68*, 1362–1367.
- (6) Baldwin, R. R.; Fuller, A. R.; Longthorn, D.; Walker, R. W. Oxidation of Formaldehyde in KCl-Coated Vessels. *J. Chem. Soc., Faraday Trans. 1* **1974**, *70*, 1257–1268.
- (7) Vardanyan, I. A.; Sachyan, G. A.; Nalbandyan, A. B. Kinetics and Mechanism of Formaldehyde Oxidation. *Combust. Flame* **1971**, *17*, 315–322.
- (8) Hochgreb, S.; Yetter, R. A.; Dryer, F. L. The Oxidation of CH₂O in the Intermediate Temperature Range (943–995 K). *Symp. Combust., [Proc.]* **1991**, *23*, 171–177.
- (9) Hochgreb, S.; Dryer, F. L. A Comprehensive Study on CH₂O Oxidation Kinetics. *Combust. Flame* **1992**, *91*, 257–284.
- (10) Glarborg, P.; Alzueta, M. U.; Kjærgaard, K.; Dam-Johansen, K. Oxidation of Formaldehyde and Its Interaction with Nitric Oxide in a Flow Reactor. *Combust. Flame* **2003**, *132*, 629–638.
- (11) Li, J.; Zhao, Z.; Kazakov, A.; Chaos, M.; Dryer, F. L.; Scire, J. J. A Comprehensive Kinetic Mechanism for CO, CH₂O, and CH₃OH Combustion. *Int. J. Chem. Kinet.* **2007**, *39* (3), 109–136.
- (12) Oldenhove de Guertechin, L.; Vandooren, J.; Van Tiggelen, P. J. Stabilisation et Analyse par Spectrométrie de Masse des Flammes Unidimensionnelles CH₂O/O₂ à Basse Pression. *J. Chim. Phys. Phys.-Chim. Biol.* **1983**, *80*, 583–594.
- (13) Vandooren, J.; de Guertechin, L. O.; Van Tiggelen, P. J. Kinetics in a Lean Formaldehyde Flame. *Combust. Flame* **1986**, *64*, 127–139.
- (14) Branch, M. C.; Sadequ, M. E.; Alfarayedhi, A. A.; Van Tiggelen, P. J. Measurements of the Structure of Laminar, Premixed Flames of CH₄/NO₂/O₂ and CH₂O/NO₂/O₂ Mixtures. *Combust. Flame* **1991**, *83*, 228–239.
- (15) Dias, V.; Duynslaeger, C.; Contino, F.; Vandooren, J.; Jeanmart, H. Experimental and Modeling Study of Formaldehyde Combustion in Flames. *Combust. Flame* **2012**, *159*, 1814–1820.
- (16) Santner, J.; Haas, F. M.; Dryer, F. L.; Ju, Y. High Temperature Oxidation of Formaldehyde and Formyl Radical: A Study of 1, 3, 5-Trioxane Laminar Burning Velocities. *Proc. Combust. Inst.* **2015**, *35*, 687–694.
- (17) Zhao, H.; Fu, J.; Haas, F. M.; Ju, Y. Effect of Prompt Dissociation of Formyl Radical on 1, 3, 5-Trioxane and CH₂O Laminar Flame Speeds with CO₂ Dilution at Elevated Pressure. *Combust. Flame* **2017**, *183*, 253–260.
- (18) Gay, I. D.; Glass, G. P.; Kistiakowsky, G. B.; Niki, H. Pyrolysis and Oxidation of Formaldehyde in Shock Waves. *J. Chem. Phys.* **1965**, *43*, 4017–4022.
- (19) Schecker, H. G.; Jost, W. Zum Homogenen Thermischen Zerfall von Formaldehyd. *Ber. Bunsenges. Phys. Chem.* **1969**, *73*, 521–526.
- (20) Dean, A. M.; Craig, B. L.; Johnson, R. L.; Schultz, M. C.; Wang, E. E. Shock Tube Studies of Formaldehyde Pyrolysis. *Symp. Combust., [Proc.]* **1979**, *17*, 577–586.
- (21) Dean, A. M.; Johnson, R. L.; Steiner, D. C. Shock-Tube Studies of Formaldehyde Oxidation. *Combust. Flame* **1980**, *37*, 41–62.
- (22) Saito, K.; Kakumoto, T.; Nakanishi, Y.; Imamura, A. Thermal Decomposition of Formaldehyde at High Temperatures. *J. Phys. Chem.* **1985**, *89*, 3109–3113.
- (23) Choudhury, T. K.; Lin, M. C. Pyrolysis of Methyl Nitrite and 1, 3, 5-Trioxane Mixtures in Shock Waves: Kinetic Modeling of the H+CH₂O Reaction Rate. *Combust. Sci. Technol.* **1989**, *64*, 19–28.
- (24) Lin, C. Y.; Wang, H. T.; Lin, M. C.; Melius, C. F. A Shock Tube Study of the CH₂O+ NO₂ Reaction at High Temperatures. *Int. J. Chem. Kinet.* **1990**, *22*, 455–482.
- (25) Eiteneer, B.; Yu, C. L.; Goldenberg, M.; Frenklach, M. Determination of Rate Coefficients for Reactions of Formaldehyde Pyrolysis and Oxidation in the Gas Phase. *J. Phys. Chem. A* **1998**, *102*, 5196–5205.
- (26) Irdam, E. A.; Kiefer, J. H.; Harding, L. B.; Wagner, A. F. The Formaldehyde Decomposition Chain Mechanism. *Int. J. Chem. Kinet.* **1993**, *25*, 285–303.
- (27) Hidaka, Y.; Taniguchi, T.; Kamesawa, T.; Masaoka, H.; Inami, K.; Kawano, H. High Temperature Pyrolysis of Formaldehyde in Shock Waves. *Int. J. Chem. Kinet.* **1993**, *25*, 305–322.
- (28) Friedrichs, G.; Davidson, D. F.; Hanson, R. K. Direct Measurements of the Reaction H+ CH₂O → H₂+ HCO behind Shock Waves by Means of Vis–UV Detection of Formaldehyde. *Int. J. Chem. Kinet.* **2002**, *34*, 374–386.
- (29) Friedrichs, G.; Davidson, D. F.; Hanson, R. K. Validation of a Thermal Decomposition Mechanism of Formaldehyde by Detection of CH₂O and HCO behind Shock Waves. *Int. J. Chem. Kinet.* **2004**, *36*, 157–169.
- (30) Vasudevan, V.; Davidson, D. F.; Hanson, R. K.; Bowman, C. T.; Golden, D. M. High-Temperature Measurements of the Rates of the Reactions CH₂O+ Ar → Products and CH₂O+ O₂ → Products. *Proc. Combust. Inst.* **2007**, *31*, 175–183.
- (31) Wang, S.; Davidson, D. F.; Hanson, R. K. High-Temperature Laser Absorption Diagnostics for CH₂O and CH₃CHO and Their Application to Shock Tube Kinetic Studies. *Combust. Flame* **2013**, *160*, 1930–1938.
- (32) Wang, S.; Dames, E. E.; Davidson, D. F.; Hanson, R. K. Reaction Rate Constant of CH₂O+ H= HCO+ H₂ Revisited: A Combined Study of Direct Shock Tube Measurement and Transition State Theory Calculation. *J. Phys. Chem. A* **2014**, *118*, 10201–10209.
- (33) Davidson, D. F.; Herbon, J. T.; Horning, D. C.; Hanson, R. K. OH Concentration Time Histories in n-Alkane Oxidation. *Int. J. Chem. Kinet.* **2001**, *33*, 775–783.
- (34) Wang, S.; Davidson, D. F.; Hanson, R. K. High Temperature Measurements for the Rate Constants of C₁–C₄ Aldehydes with OH in a Shock Tube. *Proc. Combust. Inst.* **2015**, *35*, 473–480.
- (35) Hochgreb, S.; Dryer, F. L. Decomposition of 1, 3, 5-Trioxane at 700–800 K. *J. Phys. Chem.* **1992**, *96*, 295–297.
- (36) Ren, W.; Farooq, A.; Davidson, D. F.; Hanson, R. K. CO Concentration and Temperature Sensor for Combustion Gases using Quantum-Cascade Laser Absorption near 4.7 μm. *Appl. Phys. B: Lasers Opt.* **2012**, *107*, 849–860.
- (37) Herbon, J. T. Shock Tube Measurements of CH₃+O₂ Kinetics and the Heat of Formation of the OH Radical. Ph.D. Dissertation, Stanford University: Stanford, CA, June 2004.
- (38) Li, Y.; Zhou, C. W.; Somers, K. P.; Zhang, K.; Curran, H. J. The Oxidation of 2-Butene: A High Pressure Ignition Delay, Kinetic

- Modeling Study and Reactivity Comparison with Isobutene and 1-Butene. *Proc. Combust. Inst.* **2017**, *36*, 403–411.
- (39) Smith, G. P.; Golden, D. M.; Frenklach, M.; Moriarty, N. W.; Eiteneer, B.; Goldenberg, M.; Bowman, C. T.; Hanson, R. K.; Song, S.; Gardiner, W. C., Jr., et al. *GRI Mech Version 3.0*, available at http://www.me.berkeley.edu/gri_mech/, July 1999.
- (40) Wang, H.; You, X.; Joshi, A. V.; Davis, S. G.; Laskin, A.; Egolfopoulos, F.; Law, C. K. *USC Mech Version II*, available at http://ignis.usc.edu/USC_Mech_II.htm, May 2007.
- (41) Christensen, M.; Nilsson, E. J. K.; Konnov, A. A. A Systematically Updated Detailed Kinetic Model for CH_2O and CH_3OH Combustion. *Energy Fuels* **2016**, *30*, 6709–6726.
- (42) Ruscic, B.; Wagner, A. F.; Harding, L. B.; Asher, R. L.; Feller, D.; Dixon, D. A.; Peterson, K. A.; Song, Y.; Qian, X.; Ng, C. Y.; et al. On the Enthalpy of Formation of Hydroxyl Radical and Gas-Phase Bond Dissociation Energies of Water and Hydroxyl. *J. Phys. Chem. A* **2002**, *106*, 2727–2747.
- (43) Herbon, J. T.; Hanson, R. K.; Golden, D. M.; Bowman, C. T. A Shock Tube Study of the Enthalpy of Formation of OH. *Proc. Combust. Inst.* **2002**, *29*, 1201–1208.
- (44) Dreier, T.; Wolfrum, J. Direct Study of the Reaction of vibrationally Excited CO Molecules with OH Radicals. *Symp. Combust., [Proc.]* **1981**, *18*, 801–809.
- (45) Wooldridge, M. S.; Hanson, R. K.; Bowman, C. T. A Shock Tube Study of the $\text{CO} + \text{OH} \rightarrow \text{CO}_2 + \text{H}$ Reaction. *Symp. Combust., [Proc.]* **1994**, *25*, 741–748.
- (46) Hong, Z.; Davidson, D. F.; Barbour, E. A.; Hanson, R. K. A New Shock Tube Study of the $\text{H} + \text{O}_2 \rightarrow \text{OH} + \text{O}$ Reaction Rate Using Tunable Diode Laser Absorption of H_2O near $2.5 \mu\text{m}$. *Proc. Combust. Inst.* **2011**, *33*, 309–316.
- (47) Urzay, J.; Kseib, N.; Davidson, D. F.; Iaccarino, G.; Hanson, R. K. Uncertainty-Quantification Analysis of the Effects of Residual Impurities on Hydrogen–Oxygen Ignition in Shock Tubes. *Combust. Flame* **2014**, *161*, 1–15.
- (48) Wang, S.; Davidson, D. F.; Hanson, R. K. Improved Shock Tube Measurement of the $\text{CH}_4 + \text{Ar} = \text{CH}_3 + \text{H} + \text{Ar}$ Rate Constant using UV Cavity-Enhanced Absorption Spectroscopy of CH_3 . *J. Phys. Chem. A* **2016**, *120*, 5427–5434.
- (49) George, M. A.; Kiefer, J. H.; Hessler, J. P. Removal of Simple Hydrocarbons from a Rare Gas by a 70% Zr-25% V-5% Fe Getter. *Gas Sep. Purif.* **1989**, *3*, 50–55.
- (50) Rea, E. C.; Chang, A. Y.; Hanson, R. K. Shock-Tube Study of Pressure Broadening of the $\text{A}^2\Sigma^+ - \text{X}^2\Pi(0, 0)$ Band of OH by Ar and N_2 . *J. Quant. Spectrosc. Radiat. Transfer* **1987**, *37*, 117–127.
- (51) Sutherland, J. W.; Michael, J. V.; Pirraglia, A. N.; Nesbitt, F. L.; Klemm, R. B. Rate Constant for the Reaction of $\text{O}(^3\text{P})$ with H_2 by the Flash Photolysis—Shock Tube and Flash Photolysis—Resonance Fluorescence Techniques; $504\text{K} \leq T \leq 2495\text{K}$. *Symp. Combust., [Proc.]* **1988**, *21*, 929–941.
- (52) Friedrichs, G.; Herbon, J. T.; Davidson, D. F.; Hanson, R. K. Quantitative Detection of HCO behind Shock Waves: The Thermal Decomposition of HCO. *Phys. Chem. Chem. Phys.* **2002**, *4*, 5778–5788.
- (53) Lam, K. Y.; Davidson, D. F.; Hanson, R. K. A Shock Tube Study of $\text{H}_2 + \text{OH} \rightarrow \text{H}_2\text{O} + \text{H}$ using OH Laser Absorption. *Int. J. Chem. Kinet.* **2013**, *45*, 363–373.
- (54) Smith, G. P.; Tao, Y.; Wang, H. Foundational Fuel Chemistry Model Version 1.0 (FFCM-1), available at <http://nanoenergy.stanford.edu/ffcm>, 2016.
- (55) Joshi, A. V.; Wang, H. Master Equation Modeling of Wide Range Temperature and Pressure Dependence of $\text{CO} + \text{OH} \rightarrow$ Products. *Int. J. Chem. Kinet.* **2006**, *38*, 57–73.